Available online at www.sciencedirect.com
SCIENCE DIRECT®
Acta Biomaterialia 1 (2005) 5–13
Acta BIOMATERIALIA
www.actamat-journals.com

Adhesion design maps for bio-inspired attachment systems

Ralph Spolenak, Stanislav Gorb, Eduard Arzt *

Max Planck-Institute for Metals Research, Heisenbergstr. 3, D-70569 Stuttgart, Germany

Received 3 June 2004; received in revised form 20 August 2004; accepted 27 August 2004

Abstract

Fibrous surface structures can improve the adhesion of objects to other surfaces. Animals, such as flies and geckos, take advantage of this principle by developing "hairy" contact structures which ensure controlled and repeatable adhesion and detachment. Mathematical models for fiber adhesion predict pronounced dependencies of contact performance on the geometry and the elastic properties of the fibers. In this paper the limits of such contacts imposed by fiber strength, fiber condensation, compliance, and ideal contact strength are modeled for spherical contact tips. Based on this, we introduce the concept of "adhesion design maps" which visualize the predicted mechanical behavior. The maps are useful for understanding biological systems and for guiding experimentation to achieve optimum artificial contacts.

Keywords: Attachment; Adhesion; Dry adhesives; Locomotion; JKR theory; Contact mechanics; Elasticity; Surface patterning; Young's modulus; Shapes; Materials selection; Design

1. Introduction

Molecular adhesion of solid objects mediated by van der Waals forces plays an important role in everyday life and in several branches of technology. Examples are the adhesion of sticky tapes to smooth surfaces [1], the grip of racing car tires on the race course surface [2], silicon wafer bonding [3] or the undesirable coagulation of micro-objects in the packaging industry (referred to as "stiction") [4]. Common to all these cases is the formation of mechanical contact without chemical bonding but with a defined minimum stress required for the separation of the objects. Making and breaking of the contact is usually reversible and does not lead to permanent changes in the objects involved. Nature makes use of this phenomenon for rapidly releasable mechanical contacts to unpredictable surfaces with random properties. A case in point is the adhesion of various animals, e.g. beetles, flies, spiders, and geckos, to surfaces during locomotion [5–11]. Recently, experimental evidence has been found [12] that the adhesion of geckos relies indeed on van der Waals forces. In beetles, flies and spiders, these "molecular" forces at least contribute strongly (but are reinforced by additional effects, such as the secretion of oily fluids) [13–16]. The promise of transferring new insight gained on natural adhesion systems to artificial contact devices has spurred much research activity in this field in recent years [12,17–24].

In the hypothetical case of ideally matching, smooth surfaces, van der Waals bonds can create separation stresses (or "pull-off stresses") of appreciable magnitude. This theoretical contact strength is easily estimated as

$$\sigma_{\text{th}} \approx \frac{\gamma}{b} \tag{1}$$

Here $\gamma = \gamma_1 + \gamma_2 - \gamma_{12}$ is the work of adhesion where γ_1 and γ_2 are the specific surface energies of the two bodies in contact and γ_{12} is the specific energy of the interface

* Corresponding author.
E-mail addresses: spolenak@mf.mpg.de (R. Spolenak), s.gorb@mf.mpg.de (S. Gorb), arzt@mf.mpg.de (E. Arzt).

1742-7061/$ - see front matter
doi:10.1016/j.actbio.2004.08.004

Table 1
Symbols

A_{app}	apparent contact area (m^2)
C	numerical factor (–)
B	length of surface interaction (m)
E	Young's modulus (N/m^2)
E^*	reduced modulus (N/m^2)
E_{eff}	effective Young's modulus (N/m^2)
F	area fraction of fibers (–)
L	fiber length (m)
P_c	pull-off force of a single contact (N)
R	fiber radius (m)
Y	numerical factor (–)
γ	work of adhesion (N/m)
γ'	work of adhesion between contact tips (N/m)
γ_1, γ_2	specific surface energies (N/m)
Δ	half the inter-fiber distance (m)
λ	fiber aspect ratio (–)
ν	Poisson's ratio (–)
σ_{app}	apparent contact strength (N/m^2)
σ_c	contact strength (N/m^2)
σ_f	axial fiber stress (N/m^2)
σ_{th}	theoretical contact strength (N/m)

formed between them; b is the characteristic length of surface interaction (see also Table 1 for symbols used throughout the text). By choosing typical values ($\gamma = 50\,mJ/m^2$ and $b = 2\times10^{-10}\,m$), the theoretical pull-off stress is found to be of order 200 MPa. A similar value is obtained by setting $\sigma_{th} = E/10$ where E is Young's modulus typical of van der Waals bonding ($E \approx 2\,GPa$) [25].

Such high adhesion stresses are never encountered in real systems, mainly for two reasons: the contacting surfaces never match perfectly, which lowers the area of true contact and requires accommodating elastic deformation of one or both solids [26,27]; and the contact between a body of finite dimensions and an infinite half-space sets up stress singularities at the edges which reduce the pull-off force [28]. Applying conventional contact mechanics, it has recently been shown that in such a "non-ideal" situation the pull-off force can be increased by the principle of contact splitting [12,19,29]: many small contacts are superior to one large contact of the same total area of apparent contact. The shape of the contact elements (called "tips" below) also influences contact strength [21]. In addition, it is advantageous to compensate for the roughness of the substrate by creating contact structures with high compliance, e.g. by placing the contact tips at the ends of fibers with high aspect ratios. In the course of evolution, nature has repeatedly developed such "hairy" attachment structures (Fig. 1). Their size reflects in a quantitative way the principle of contact splitting as heavier animals from different lineages display progressively finer contact tips [19].

Largely through "bio-inspiration" and trial and error, artificial contact systems have recently been designed in the laboratory [12,18,22,23,30,31]. However, a thorough understanding of the adhesion of fiber structures is required for a more rational approach. Several recent papers have treated different theoretical aspects of the contact problem [20–22,24,32]. While these views do not yet fully converge, it is apparent from these studies that the performance of an adhesive contact depends critically on a multitude of parameters; the most important are size and shape of the contact tips and the elastic properties of the fibers and their tips. In this paper we introduce the concept of an "adhesion design map" which delineates the mechanical limits of fiber contacts according to our current understanding. The maps will be discussed with reference to biological contact devices. It will be proposed that they can be used as convenient guidelines for improving contact strength in artificial adhesion systems.

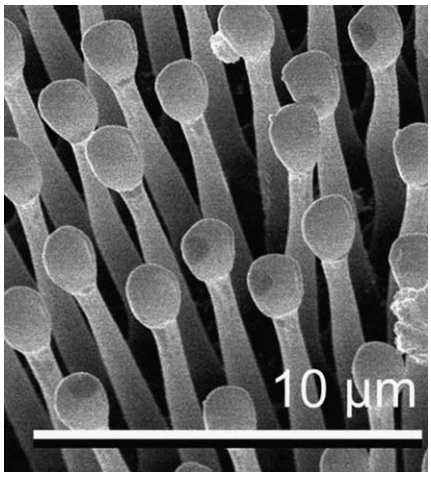

Fig. 1. Scanning electron micrograph of the attachment system of the fly *Calliphora vicina*.

2. Mechanical limits of fiber contacts

Consider an adhesive structure consisting of parallel fibers with radius R, length L and inter-fiber distance 2Δ (Fig. 2). The tip shape is assumed to be hemispherical with radius R. The material properties, i.e. Young's modulus E of the fibers and their tips, are identical and homogeneous. The substrate is ideally flat and has infinite stiffness. We assume further that the Johnson–Kendall–Roberts (JKR) theory [26] can be applied [21]. The force P_c for pull-off of a single spherical tip is then given by:

$$P_c = \tfrac{3}{2}\pi\gamma R \tag{2}$$

The apparent contact strength σ_{app} is defined as the pull-off force divided by the apparent contact area A_{app}:

$$\sigma_{app} = \frac{P_c}{A_{app}} = \frac{3f\gamma}{2R} \tag{3}$$

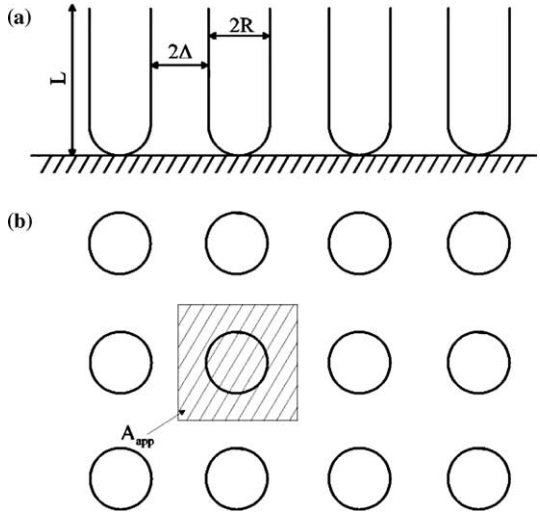

Fig. 2. Schematic of a fibrous attachment system in side view (a) and in plan view (b). The fibers are cylindrical with length L, radius R, and interfiber distance 2Λ. The aspect ratio λ is defined as $(L/2R)$. The apparent contact area of a single fiber is shown as a shaded square.

Here, f is the area fraction of fibers, which is given by

$$f = \frac{R^2\pi}{A_{\text{app}}} \tag{4}$$

Note that the contact strength scales inversely with tip radius in accordance with the principle of contact splitting. However, progressive miniaturization of the contact tips is limited by other mechanisms, as will now be shown.

2.1. The limit of fiber fracture

For sufficiently fine contacts, the strength of the system will eventually be determined by fracture of the fibers. The axial stress σ_f in a fiber is limited by its theoretical fracture strength $\sigma_{\text{th}}^{\text{f}}$ such that:

$$\sigma_{\text{f}} = \frac{P_{\text{c}}}{R^2\pi} \leqslant \sigma_{\text{th}}^{\text{f}} \tag{5}$$

Inserting Eq. (2) gives a lower limit for the useful fiber radius R:

$$R \geqslant \frac{3\gamma}{2\sigma_{\text{th}}^{\text{f}}} \approx \frac{15\gamma}{E} \tag{6}$$

where we have approximated the theoretical fracture strength by $E/10$.

Thinner fibers than given by Eq. (6) result in fiber fracture rather than contact detachment. As this failure mechanism depends on the actual contact area, the apparent fracture strength is then no longer affected by contact splitting. It is therefore impractical to refine the fibers beyond the radius given by Eq. (6).

2.2. The limit of ideal contact strength

The contact strength cannot exceed the ideal contact strength transmitted through the actual contact area at the instant of tensile instability. This condition can be expressed as

$$\sigma_{\text{c}} = \frac{P_{\text{c}}}{a_{\text{c}}^2\pi} \leqslant \sigma_{\text{th}} \tag{7}$$

where σ_{c} is the contact strength and σ_{th}, the ideal strength of van der Waals bonds as given in Eq. (1). The contact radius a_{c} at the instant of pull-off (at $P = P_{\text{c}}$) can be calculated from the JKR theory [26]:

$$a_{\text{c}} = \left(\frac{9\pi\gamma R^2}{8E^*}\right)^{1/3} \tag{8}$$

where E^* is the reduced modulus of the fiber/substrate system with the Young's moduli E and E_{s} and Poisson's numbers ν and ν_{s}:

$$\frac{1}{E^*} = \frac{1-\nu^2}{E} + \frac{1-\nu_{\text{s}}^2}{E_{\text{s}}} \tag{9}$$

For an infinitely stiff substrate, as assumed here, the second term in this equation vanishes. Combining Eqs. (2) and (7)–(9) and solving for R yields:

$$R \geqslant \frac{b^3E^2}{Y\gamma^2} \tag{10}$$

where Y is a numerical factor

$$Y = \frac{3\pi^2}{8}(1-\nu^2)^2 \tag{11}$$

which amounts to 3.06 (for $\nu = 0.3$).

Eq. (10) sets a lower bound on the fiber radius R, which corresponds to an upper bound for Young's modulus E. Although the modulus does not enter in the JKR pull-off stress (Eq. (2)), it affects the limit of ideal contact strength in the following way: stiff contact tips exhibit, according to Eq. (8), smaller contacts at pull-off, which leads to lower ideal pull-off forces.

For future reference it is convenient to express the condition for constant apparent contact strength in the regime outside that given by Eq. (10). Combining Eqs. (1), (3), (4), (7) and (8) results in:

$$\sigma_{\text{app}} = \frac{f\gamma^{5/3}}{4bE^{2/3}R^{2/3}}[9\pi(1-\nu^2)]^{2/3} \tag{12}$$

Compared to Eq. (3), the beneficial effect of reducing the tip radius R is now reduced. Note also that in this regime the Young's modulus E enters in the apparent contact strength.

2.3. The limit of fiber condensation

When the adhesive forces between the contact tips become stronger than the forces required to bend the

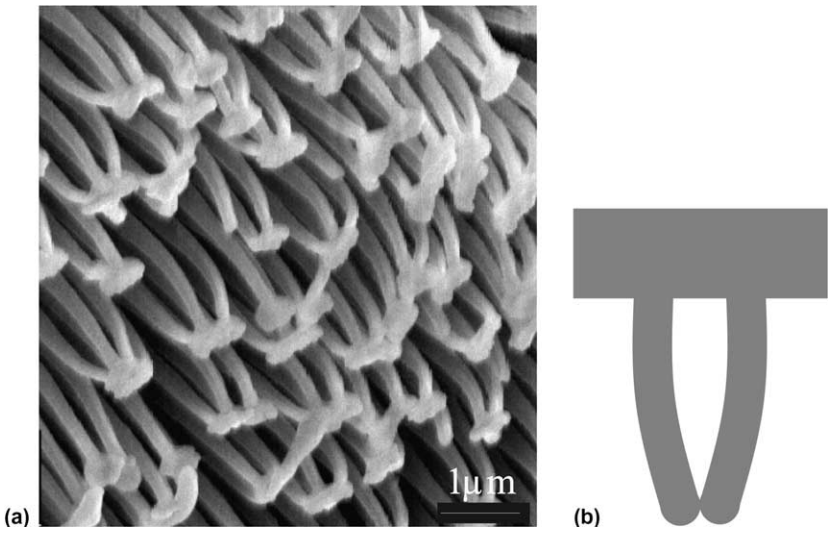

Fig. 3. Fiber condensation: (a) scanning electron micrograph of the hairy attachment system of the spider *Aphonopelma seemanii* showing condensation of the contact tips; (b) schematic of fiber condensation.

fibers, the fibers will tend to condensate as shown in Fig. 3. Several authors [20,22,33] have formulated a condensation criterion. We adopt the approach of Sitti and Fearing [22], who modeled the fibers as elastic beams whose tips are attracted by a force F. The force required to bend a fiber to a tip displacement Δ is

$$F = \frac{3\pi R^4 E \Delta}{4L^3} \tag{13}$$

Equating this expression to the JKR pull-off force for two spherical tips [26] results in the following criterion for avoiding condensation:

$$R \geqslant \frac{8\gamma' h(f)^{1/2}}{E}\lambda^3 \tag{14}$$

where λ is the aspect ratio of a fiber defined as $(L/2R)$. Here γ' denotes the work of adhesion between two fiber tips, which may differ numerically from γ. The function $h(f)$ is given by:

$$\frac{1}{h(f)} = \left(\sqrt{\frac{\pi}{4f}} - 1\right)^2 \tag{15}$$

The condition Eq. (14) not only contains the fiber radius R, but additionally its aspect ratio λ. It places an upper bound on the aspect ratio to prevent fiber condensation, which is detrimental as it counteracts the benefits of contact splitting and impairs the adaptability of the contact structure.

2.4. The limit of contact adaptability

In order to enable adhesion to rough surfaces, a minimum elastic adaptability of the fiber structure is required. In addition, the energetics of contact formation requires that the elastic strain energy stored in the structure during contact be smaller than the work of adhesion [20]. These requirements can be met by setting an upper limit on the "effective" modulus of the fiber structure. To avoid the buckling instability, we consider a fiber array that meets the substrate at an angle and is therefore stressed in a bending mode. We use Persson's result [20] for the effective modulus, which prescribes an upper bound on the fiber modulus:

$$E < E_{\text{eff}} \frac{4\pi}{Cf}\lambda^2 \tag{16}$$

Here E_{eff} is an assumed value for the structural modulus to ensure contact adaptability. C is a geometrical factor of the order 10 [20]. Limiting the effective modulus to a specific value, e.g. $E_{\text{eff}} = 1\,\text{MPa}$, places either an upper bound on Young's modulus of the fiber material or a lower bound on the aspect ratio λ. The choice of E_{eff} is somewhat arbitrary and will depend e.g. on the roughness of the substrate.

3. Introduction of adhesion design maps

The mathematical descriptions of the limiting conditions for fibrous adhesion structures will now be visualized graphically. For this purpose we introduce the concept of an "adhesion design map". We first describe the construction and the characteristics of these maps and study their sensitivity to changes in the input parameters. Then, the potential of the maps for predicting the parameters of optimum contact structures will be outlined. Finally, the design maps will be compared with typical data for biological systems.

3.1. Construction of the maps

The most fundamental fiber properties are their radius R and their Young's modulus E. We propose a double-logarithmic plot in R–E space. Values for other input parameters, such as the work of adhesion γ and the fiber area fraction f, will be preset at specific values for a given map. Fig. 4 displays a first map which illustrates the principle. Two limiting conditions are plotted as heavy lines: the onset of fiber fracture corresponds to a line of slope −1 (following Eq. (6)), whereas the criterion of ideal contact strength follows a slope of 2 (Eq. (10)). Contours of constant apparent contact strength are shown as fine lines. According to the principle of contact splitting (Eq. (3)), these lines conform to increasing contact strength with decreasing tip radius. The arrow marks the direction of increasing apparent contact strength. Below the "fiber fracture" condition, however, the contours are deflected vertically, because here contact performance can no longer be improved by contact splitting. Similarly, the contacts are weakened below the "ideal contact strength" limit, which results in a reduced slope of the contours (slope −1 following Eq. (12)). As no or only a diminished gain is predicted from contact sizes below the heavy lines in Fig. 4, these regions should be avoided in the design of artificial systems.

A full adhesion design map which includes all four limiting conditions is depicted in Fig. 5. The "condensation" limit results in lines with the same slope as the "fiber fracture" limit; its absolute position however shifts with the aspect ratio λ and area fraction f (Eq. (14)). The "adaptability" criterion produces vertical cut-offs also related to both parameters (Eq. (16)). Fulfilling all of these requirements, including a minimum apparent contact strength, results typically in a triangular target area (shaded in Fig. 5). The position of this triangle shifts with the value of the aspect ratio (chosen here as $\lambda = 10$).

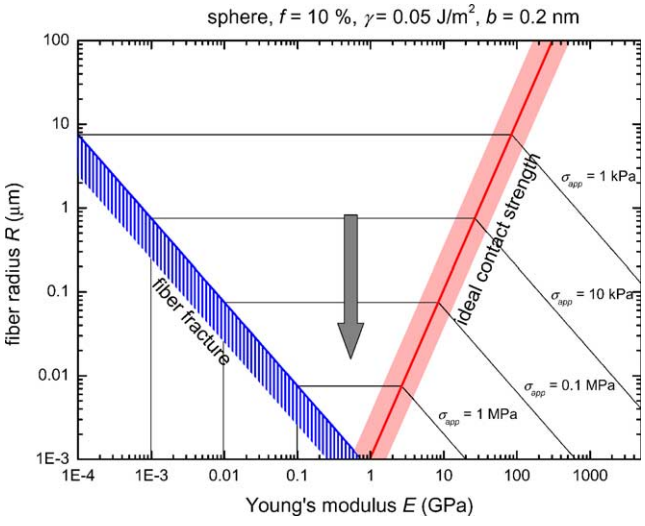

Fig. 4. Partial adhesion design map for spherical tip shape. The following parameters are assumed: $\gamma = 0.05\,J/m^2$, $f = 10\%$, $b = 0.2\,nm$. The criteria for fiber fracture (blue line) and ideal contact strength (red line) are indicated. Thin lines are contours of equal apparent contact strength. The arrow indicates the direction of increasing apparent contact strength.

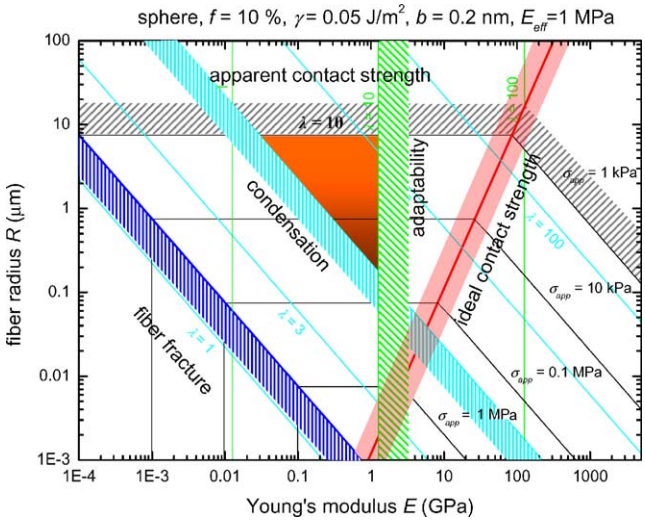

Fig. 5. Adhesion map with the same parameters as in Fig. 4 but including the criteria of condensation (cyan lines) and adaptability (green lines). The triangular target area delineates the allowed parameter space for an adhesive structure with an aspect ratio $\lambda = 10$ and a required apparent contact strength of at least 1 kPa.

Figs. 6 and 7 show the dependence of the design maps on the work of adhesion γ and the area fraction f. A reduction in work of adhesion (Fig. 6a) shifts the "fiber fracture" criterion, the "ideal contact" strength and the "condensation criterion" to lower moduli. As the "adaptability" criterion remains unchanged the triangular target area shifts to smaller fiber radii with decreasing work of adhesion. The converse is true for higher work of adhesion (Fig. 6b).

Changing the area fraction f influences the "condensation" and the "adaptability criterion" and the contours of apparent contact strength. The "fiber fracture" condition and the "ideal contact strength" remain unchanged (Fig. 7a and b). With decreasing area fraction, the target triangle shifts to higher moduli and smaller fiber radii. In Fig. 7b it has even transgressed the "ideal contact strength" limit.

3.2. Prediction of optimum adhesive contacts

The adhesion design maps narrow down the useful range of Young's moduli for the fibers and tips to produce optimum contact. If only the two criteria "fiber fracture" and "ideal contact strength" were to be considered (as in Fig. 4), the Young's modulus should come

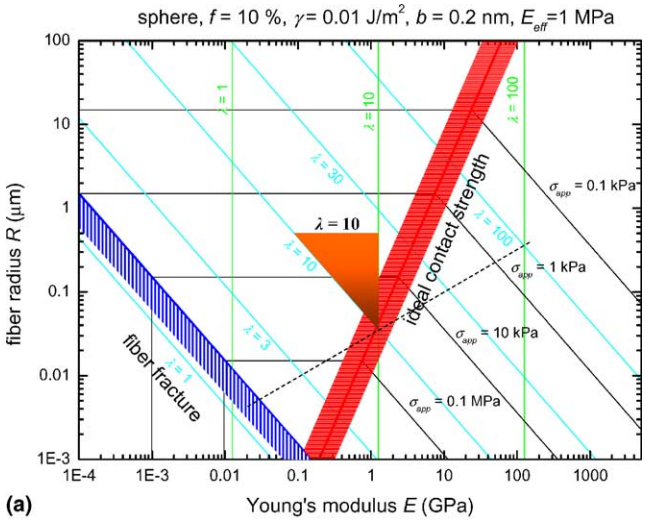

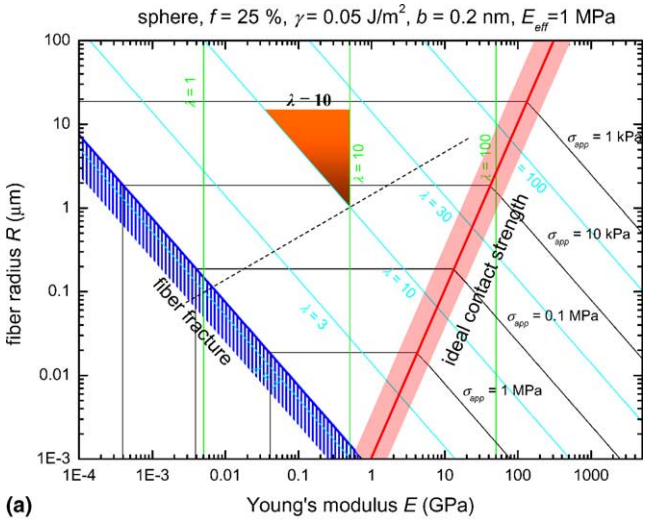

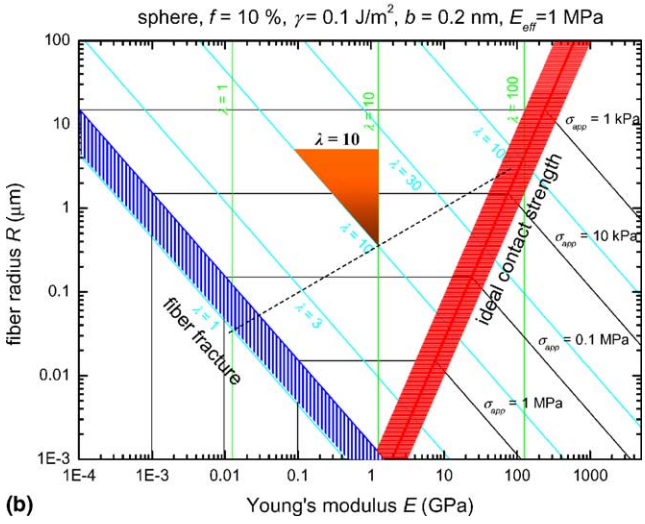

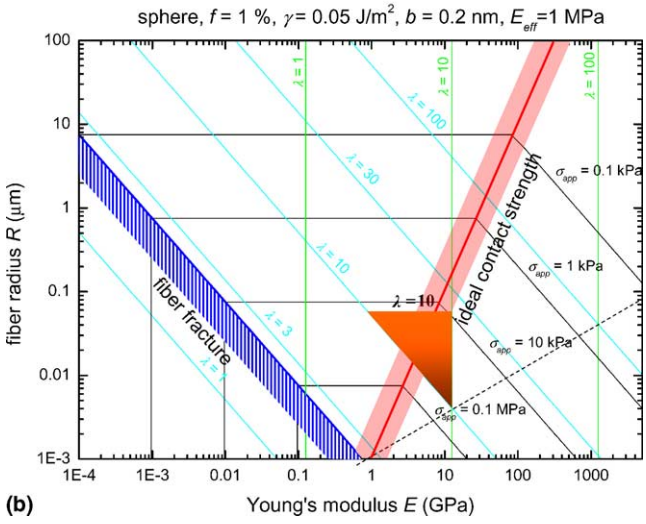

Fig. 6. Same as Fig. 5 but varying the work of adhesion: (a) $\gamma = 0.01\,\mathrm{J/m^2}$ and (b) $\gamma = 0.1\,\mathrm{J/m^2}$. The broken line is a "conode" which links loci of optimum contact strength for different fiber aspect ratios.

Fig. 7. Same as Fig. 5 but varying the area fraction of fibers: (a) $f = 25\%$ and (b) $f = 1\%$.

to lie in the cusp formed by the two heavy lines, i.e. at their intersection. This condition is expressed as:

$$\widehat{E} = \frac{(15Y)^{1/3}\gamma}{b} \approx 3.5\frac{\gamma}{b} \tag{17}$$

It is interesting that this critical modulus is of the same order of magnitude as the ideal contact strength given in Eq. (1). Because of the comparatively weak van der Waals bonding at the contact, this means that materials for contact tips should also exhibit low modulus typical of van der Waals-dominated or elastomeric (entropy-dominated) materials.

Eq. (17) prescribes a critical tip radius given by

$$\widehat{R} = \frac{15^{2/3}b}{Y^{2/3}} \approx 4.2b \tag{18}$$

Using Eq. (3) and substituting Eq. (1) would then give an apparent contact strength of

$$\hat{\sigma}_{\mathrm{app}} = \left(\frac{3Y^{1/3}}{2\times 15^{2/3}}\right)\frac{f\gamma}{b} \approx 0.35 f\sigma_{\mathrm{th}} \tag{19}$$

For high area fractions f, an appreciable fraction of the theoretical strength would therefore be expected. These considerations are however in most cases hypothetical, as the "condensation" and "adaptability" criteria will intervene.

Among the two criteria "fiber strength" or "condensation" (which show up as parallel lines in the diagrams), it is usually the "condensation" limit which is the more stringent requirement. Comparing the tip radii given in Eqs. (6) and (14) leads to the following condition for the condensation limit to lie above the fiber strength limit:

$$\lambda > \left(\frac{15\gamma}{8\gamma'}\right)^{1/3}\frac{1}{h(f)^{1/6}} \tag{20}$$

For reasonable assumptions, this lower bound on the aspect ratio is usually fulfilled. Hence the condensation limit will in most cases control how fine the fibers can be made. This conclusion would however not be valid if the strength of the fiber material were not equal to the theoretical fracture strength as was assumed in the derivation of Eq. (6).

We can now attempt to predict the requirements for the ultimate fiber adhesion structure. Within the triangular target areas shown in Figs. 5–7, the apparent contact strength is maximized at their lower apex. When this triangle is plotted for different aspect ratios λ, these apices come to lie on a straight line with slope 1/2. We call this line, which is shown in Figs. 6–8, the "conode".

The ultimate limit for the apparent contact strength is located at the intersection of the conode with the line marking the "fiber fracture" limit. This ideal locus is marked with a red circle in Fig. 8. Its position can be mathematically found by requiring the criteria Eqs. (6), (14) and (16) to coincide. This leads to the following prediction for the optimum fiber tip radius:

$$R_{\mathrm{opt}} = \frac{C \times 15^{1/3}}{\pi} \frac{\gamma^{1/3}\gamma'^{2/3} f h(f)^{1/3}}{E_{\mathrm{eff}}} \approx \frac{7.8\gamma^{1/3}\gamma'^{2/3} f h(f)^{1/3}}{E_{\mathrm{eff}}} \tag{21}$$

under the condition that this value does not lie below $\widehat{R}$ given by Eq. (18). The corresponding Young's modulus is given by:

$$E_{\mathrm{opt}} = \frac{15^{2/3}\pi}{C}\left(\frac{\gamma}{\gamma'}\right)^{2/3} \frac{E_{\mathrm{eff}}}{f h(f)^{1/3}} \approx 1.9\left(\frac{\gamma}{\gamma'}\right)^{2/3} \frac{E_{\mathrm{eff}}}{f h(f)^{1/3}} \tag{22}$$

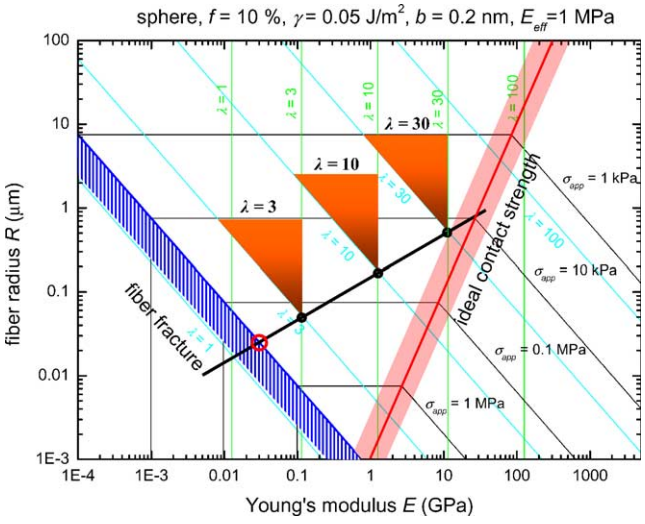

Fig. 8. Same as Fig. 5, displaying the line which connects the optimum loci for different aspect ratios λ ("conode", thick black line). The red circle indicates the optimum solution.

under the condition that this value does not exceed $\widehat{E}$ given by Eq. (17). Eqs. (21) and (22) also define an optimum aspect ratio:

$$\lambda_{\mathrm{opt}} = \frac{15^{1/3}}{2}\left(\frac{\gamma}{\gamma'}\right)^{1/3} \frac{1}{h(f)^{1/6}} \approx 1.2\left(\frac{\gamma}{\gamma'}\right)^{1/3} \frac{1}{h(f)^{1/6}} \tag{23}$$

The ultimate apparent contact strength is obtained by inserting Eq. (21) into Eq. (3):

$$\sigma_{\mathrm{app}}^{\mathrm{opt}} = \left(\frac{3\pi}{2C15^{1/3}}\right)\left(\frac{\gamma}{\gamma'}\right)^{2/3} \frac{E_{\mathrm{eff}}}{h(f)^{1/3}} \tag{24}$$

under the condition that this value does not exceed Eq. (19). It is interesting to note that the ultimate contact strength is independent of γ (for $\gamma = \gamma'$) and depends linearly on E_{eff}. As expected, flat surfaces, for which large values of the effective modulus can be allowed, will enable better attachment. It is rather counter-intuitive that *low* values of $h(f)$, i.e. low fiber fractions, favor attachment. With reference to Fig. 7a and b, this may be explained as follows: for lower area fractions, the "adaptability" criterion moves to larger values of E and the "condensation" criterion to smaller R values. Hence their point of intersection, i.e. the triangle apex, comes to lie at progressively smaller tip radii, which results in higher apparent contact forces. Because of the cube-root dependence in Eq. (24), this effect is however rather weak.

It is instructive to estimate the optimum numerical values based on these equations. Assuming $\gamma = \gamma' = 50\,\mathrm{mJ/m^2}$, $E_{\mathrm{eff}} = 1\,\mathrm{MPa}$ and $f = 0.1$ results in tip radii of about 26 nm and optimum Young's moduli of about 28 MPa (as is also seen in Fig. 8). Further optimum values for different values of γ, E and f are listed in Table 2. It is readily seen that the tip radius R_{opt} scales with the work of adhesion γ, which however has no effect on the Young's modulus E_{opt} or on the aspect ratio λ_{opt}. The effective modulus E_{eff} determines the values of E_{opt}, but again does not influence λ_{opt}. The tip radius R_{opt} is inversely related to E_{eff}. The optimum aspect ratio λ_{opt} depends mainly on the area fraction f, and lies between about 1.1 (for $f = 0.25$) and 2.4 (for $f = 0.01$).

Finally, we address the question under which optimum condition the conode passes through the cusp defined by Eqs. (17)–(19). Combining these equations with Eqs. (21)–(24) gives the following requirement:

$$\gamma\gamma'^2 = \left(\frac{15\pi^3}{C^3 Y}\right)\left(\frac{bE_{\mathrm{eff}}}{f}\right)^3 \frac{1}{h(f)} \tag{25}$$

When this equation is fulfilled, the apparent contact strength reaches its overall optimum given by Eq. (19). It is readily seen that the contact parameters chosen for Fig. 7b come close to this point. Fig. 9 shows the dependence of the effective modulus on the area fraction at the optimum defined by Eq. (25). The non-linear dependence emphasizes the importance of surface

Table 2
Optimum contact parameters predicted according to Eqs. (17)–(24) (using $\gamma = \gamma'$, $C = 10$, and $b = 0.2\,\text{nm}$)

γ (J/m^2)	0.05	0.05	0.05	0.01	0.01	0.05
E_{eff} (Mpa)	1	1	1	1	0.1	0.1
F	0.25	0.01	0.1	0.25	0.25	0.25
$h(f)$	1.8	0.016	0.31	1.68	1.68	1.68
λ_{opt}	1.1	2.4	1.5	1.1	1.1	1.1
E_{opt} (MPa)	6.4	750	28	6.4	0.6	0.6
$\widehat{E}$ (MPa)	875	875	875	175	175	875
R_{opt} (nm)	120	1	26	23	2300	1200
$\hat{\sigma}_{\text{app}}$ (kPa)	21,875	875	8750	4375	4375	21,875
$\sigma_{\text{app}}^{\text{opt}}$ (kPa)	160	750	280	160	16	16

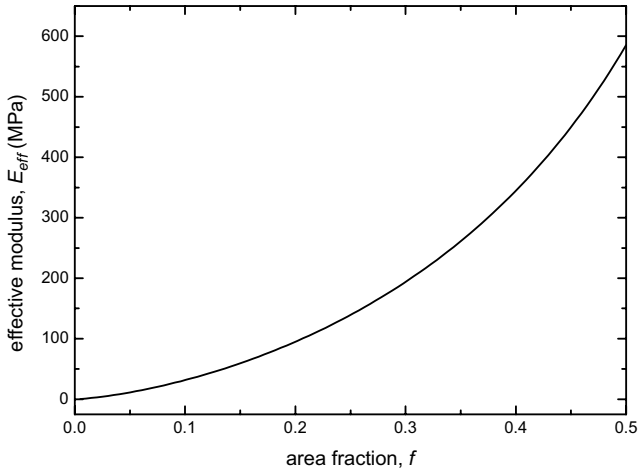

Fig. 9. The effective modulus E_{eff} vs. the area fraction f for the optimum condition given in Eq. 25 for $\gamma = \gamma' = 0.05\,\text{J/m}^2$ and $b = 0.2\,\text{nm}$.

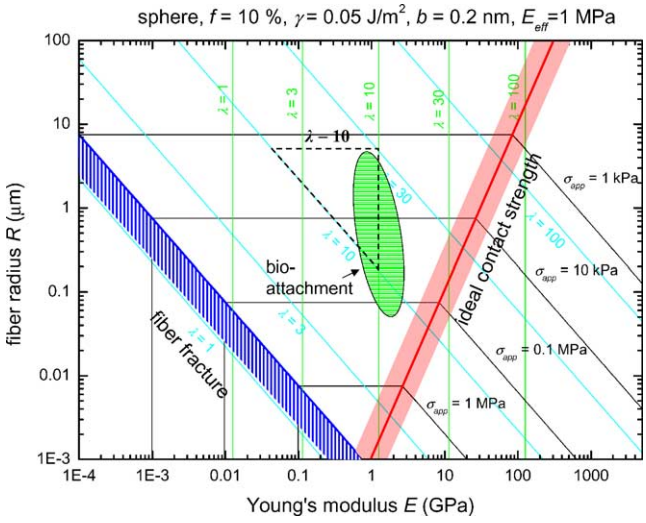

Fig. 10. The parameter range for biological contact elements (flies, beetles, spiders, and lizards), superimposed on the map of Fig. 5.

roughness for the obtainable contact strength: smooth surfaces allow high effective moduli, which require high area fractions. The optimum apparent contact strength then increases linearly with f.

3.3. First comparisons with biological adhesion systems

A preliminary attempt is made now to compare the adhesion design maps with actual data of biological attachment systems. In Fig. 10, the parameter range for contact setae or spatulae in flies, beetles, spiders and geckos is superimposed on the map of Fig. 8. The tip radii were obtained by detailed microscopy, whereas bulk values of Young's modulus [34–36] were used. It is striking that despite the simplifications made in the analysis leading to the maps, the comparison is quite promising. These biological attachment devices come to lie in the optimum region if an aspect ratio of about 10 is assumed. The quantitative agreement in apparent contact strength is also quite astonishing: flies (which are located close to the center of the region marked in Fig. 9) lie near the contour for $\sigma_{\text{app}} = 10\,\text{kPa}$; detailed analysis of pulvillus (foot) area for many different fly families has recently revealed that in order to sustain their body weight on the ceiling, an apparent contact strength of about 6 kPa is necessary [37].

One discrepancy is however worth noting: the aspect ratios of biological systems (see Figs. 1 and 3a) greatly exceed the "optimum" values predicted by Eq. (23). A possible reason is that in our treatment the "condensation" criterion assumes more dominance than in reality. The condensation limit could be shifted to smaller fiber radii by introducing a gradient in modulus or in cross-section along the fiber axis; higher values at the stem of the fiber would make bending more difficult while maintaining a low modulus at the tip would ensure that the other adhesion criteria are still satisfied. Whether natural systems take advantage of this effect, is currently under investigation. Other reasons could lie in different contact shapes or a stronger dominance of the "adaptability" criterion.

Finally a word of caution is necessary. While further quantitative conclusions may be tempting, it must be remembered that the adhesion design maps as they stand are based on severe simplifications. Like maps con-

structed to display the mechanisms of deformation [38] and of sintering [39], the present maps are not better than the mathematical equations used to construct them. For example, in this paper only spherical contact tips are treated; other shapes will be the subject of a separate publication [40]. Also, additional effects that may complicate the performance of biological contacts, e.g. oily secretions, capillary and viscoelastic effects, have not been considered. Further work along this line is in progress.

4. Conclusion

In this paper the mechanical limits of fibrous attachment systems which rely on molecular van der Waals forces have been discussed. Following contact mechanics considerations, mathematical equations describing limiting criteria for fiber fracture, ideal contact strength, fiber condensation and fiber adaptability were established. They were used as a basis for creating ''adhesion design maps''. These maps allow the effects of contact tip radius, Young's modulus and aspect ratio on contact strength to be visualized. Target areas can be defined which should optimize contact strength. It has been shown that the ultimate limit is achieved when all criteria are simultaneously fulfilled. This condition can be expressed mathematically; it unambiguously defines the optimum values of fiber radius, modulus and aspect ratio for given values of work of adhesion, fiber area fraction and fiber adaptability. A striking consequence of the present analysis is that low fiber fractions lead to better contact strength as it is then easier to circumvent fiber condensation. When comparing the maps with biological adhesion systems, some preliminary conclusion can be drawn. Caution must be exercised in quantitative analysis due to the inherent simplifications and assumptions. However, the maps can serve a useful purpose in better understanding biological attachment systems and in guiding the design of artificial attachment structures.

Acknowledgments

We acknowledge continuing discussion with H.J. Gao, Stuttgart. The micrograph in Fig. 3a was kindly provided by S. Niederegger.

References

[1] Creton C. MRS Bull 2003;6:434.
[2] Persson BNJ. Sliding friction: physical principles and applications. Berlin: Springer Verlag; 2000.
[3] Tong Q-Y, Gösele U. Semiconductor wafer bonding. New York: John Wiley & Sons, Inc.; 1998.
[4] Bhushan B, editor. Handbook of nanotechnology. Berlin, Heidelberg, New York: Springer; 2004. p. 983.
[5] Hiller U. Z Morphol Tiere 1968;62:307.
[6] Bauchhenss E. Zoomorphologie 1979;93:99.
[7] Stork NE. J Nat Hist 1983;17:829.
[8] Homann H. Naturwissenschaften 1957;44:318.
[9] Gorb SN. Proc Roy Soc Lond B 1998;265:747.
[10] Gorb S, Gorb E, Kastner V. J Exp Biol 2001;204:1421.
[11] Niederegger S, Gorb S, Jiao Y. J Comp Physiol A 2002;187:961.
[12] Autumn K, Sitti M, Liang YCA, Peattie AM, Hansen WR, Sponberg S, et al. PNAS 2002;99:12252.
[13] Ishii S. Appl Entomol Zool 1987;22:222.
[14] Kosaki A, Yamaoka R. Jpn J Appl Entomol Zool 1996;40:47.
[15] Attygale AB, Aneshansley J, Meinwald J, Eisner T. Zoology 2000;103:1.
[16] Voetsch W, Nicholson G, Müller R, Stierhof Y-D, Gorb S, Schwarz U. Insect Biochem Molec Biol 2002;32:1605.
[17] Autumn K, Peattie AM. Integr Comp Biol 2002;42:1081.
[18] Geim AK, Dubonos SV, Grigorieva IV, Novoselov KS, Zhukov AA, Shapoval SY. Nat Mater 2003;2:461.
[19] Arzt E, Gorb S, Spolenak R. PNAS 2003;100:10603.
[20] Persson BNJ. J Chem Phys 2003;118:7614.
[21] Spolenak R, Gorb S, Gao H, Arzt E. Proc Roy Soc London A, in press.
[22] Sitti M, Fearing RS. Proc 2002 2nd IEEE Conference on Nanotechnology (Cat. No. 02TH8630). IEEE, 2002. p. 137.
[23] Peressadko A, Gorb SN. J Adhes 2004;80:1.
[24] Jagota A, Bennison SJ. Integr Comp Biol 2002;42:1140.
[25] Dieter GE. Mechanical metallurgy. London: McGraw Hill; 1988, p. 245.
[26] Johnson KL, Kendall K, Roberts AD. Proc Roy Soc Lond A 1971;324:301.
[27] Fuller KNG, Tabor D. Proc Roy Soc Lond A 1975;345:327.
[28] Maugis D. Adhesion and rupture of elastic solids in solid state sciences. Springer; 1999, p. 234.
[29] Arzt E, Enders S, Gorb S. Z Metallkde 2002;93:345.
[30] Pfaff H. PhD thesis, unpublished, 2004.
[31] Sitti M, Fearing RS. J Adhes Sci Tech 2003;17:1055.
[32] Persson BNJ, Gorb S. J Chem Phys 2003;119:11437.
[33] Hui CY, Jagota A, Lin YY, Kramer EJ. Langmuir 2002;18:1394.
[34] Vincent JFV, Wegst UGK. Arthro Str Dev 2004;33:187.
[35] Wegst UGK, Ashby MF. Philos Mag 2004;84:2167.
[36] Cameron GJ, Wess TJ, Bonser RHC. J Struct Biol 2003;143:118.
[37] Schuppert J. PhD thesis, unpublished, 2004.
[38] Frost HJ, Ashby MF. Deformation mechanism maps. Oxford: Pergamon Press; 1982.
[39] Ashby MF. Acta Metall 1974;22:275.
[40] Spolenak R, Gorb S, Arzt E. 2004, in press.